Optimization Design of a Flux Switching Linear Rotary Permanent Magnet Machine

Kaikai Guo
School of Electrical and Information Engineering & School of Mechanical Engineering
Anhui University of Science and Technology
Huainan, China
guokai0072000@gmail.com

Youguang Guo
School of Electrical and Data Engineering

University of Technology Sydney
NSW, Australia
Youguang.guo-1@uts.edu.au

Abstract—A flux switching (FS) linear rotary permanent magnet (PM) machine (LRPMM) is presented with dual level FS structure in the paper. The NdFeB PM material magnetized in circumferential direction and Ferrite PM material magnetized in axial direction can produce high poly-magnetic effect, which can improve the torque/thrust density of the machine. In order to obtain the higher torque/thrust, lower torque/thrust ripple, lower cogging torque and detent force, a novel multi-parameter multi-objective optimization method is proposed. Eleven parameters are selected as the optimization parameters, which can be transformed into two virtual parameters by the initial 2-D finite element method analyzed data and coordinate transformation. Then the electromagnetic and structure parameter values are obtained, a prototype is manufactured. Compared with the initial topology, the experimental results confirm that the proposed method is remarkable and effective.

Keywords—Flux switching, finite element method, linear rotary permanent magnet machine, multi-parameter multi-objective optimization.

I. Introduction

Nowadays, the optimization design of permanent magnet (PM) machine is a hot topic, which has attracted many scholars' eyes. Many different algorithms, such as sequential nonlinear programming algorithm, extreme learning machine algorithm, gray wolf optimizer algorithm, multi-objective particle swarm optimization method and Cuckoo search technique, have been used to achieve the multi-objective optimization design of PM flux-intensifying motors [1], PM synchronous linear motors [2], radial-flux Halbach array PM limited angle torque motor [3], PM disc motor [4] and switched reluctance motor (SRM) [5], respectively. The design optimization of an interior permanent magnet synchronous motor (PMSM)[6] and surface-mounted PMSM [7] were carried out by considering both technical performances and economic issues, combining multi-independent-population genetic algorithm with subdomain model. The Kriging surrogate model used to optimize an electric machine was studied in [8], and the finite element method (FEM) was used to achieve the optimization value of a dual-rotor hybrid PM machine [9]. Based on the Artificial Bee Colony technique and strength Pareto evolutionary algorithm, a multi-objective optimization algorithm was proposed enabling global optimum tracking in PM traction motor design [10]. A Taguchi method for the design of line-start PMSMs was carried out by incorporating an improved regression rate methodology and a weighted factor multi-objective technique [11]. In order to solve the multi-objective optimization problems, a fuzzy inference Taguchi method was proposed to achieve the maximum thrust with minimum thrust ripple [12]. The response surface method (RSM) is often used in the multi-objective optimization process, which can improve the overall motor performances,

such as double-side linear Vernier PM motor [13]. In the process of studying motor structure optimization, some combined methods were investigated, such as the combined methods of FEM and dynamic dual-RSM, RSM and genetic algorithms, RSM and FEM, RSM and quantum-behaved PSO operator, Taguchi and RSM, RSM and sequential non-linear programming method, which were used in PM motors[14], PM type transverse flux linear motors [15], SRM [16], brushless PM motor [17], air-cored axial flux PM generator [18], surface-mounted and interior PMSM [19], flux switching (FS) PM motor [20]. The key parameter design of flux reversal linear rotary permanent magnet machine (LRPMM) was proposed and analyzed by building numerical analytical model [21].

An FS-LRPMM is proposed in the paper, the influence of single parameter on the electromagnetic characteristics of the machine is analyzed by 2-D FEM. Then, eleven parameters are selected as the optimization parameters, which are converted to different virtual parameters by the coordinate system transformation after the x coordinate standardization and the ranges of the parameters. Secondly, the cogging torque, detent force, torque/thrust and torque/thrust ripple are taken as the optimization objectives. Based on the optimization objectives and the virtual parameters, the optimization parameter values are obtained by the RSM, which can consider the influence on the electromagnetic characteristics when the motor is in rotary, linear or spiral motion by changing one parameter, the influence on electromagnetic characteristics when several structure parameters contradicted with each other, and the optimal accuracy requirements. A prototype is manufactured, and the electromagnetic characteristics are obtained from experiment test, and compared with those calculated by 3-D FEM.

II. FS-LRPMM Topology and Sensitivity Analysis

A. FS-LRPMM

Fig. 1 shows the topology of FS-LRPMM. There are three stator sections in the axial direction, and the mover salient poles are staggered by 22.5 degrees in the axial direction. NdFeB PM is magnetized in circumferential direction and U-shape Ferrite PM is magnetized in axial direction, which can generate the poly-magnetic effect.

B. Sensitivity Analysis

In order to reduce the design space and computational cost, each parameter affecting the performance of the machine is analyzed by 2-D FEM. Only the value of one parameter each time is changed in a certain proportion when other parameters take the central value of range. Eleven key design parameters of the FS-LRPMM are selected for the multi-parameter multi-target optimization. The

corresponding variation ranges of the selected design parameters are listed in Table I.
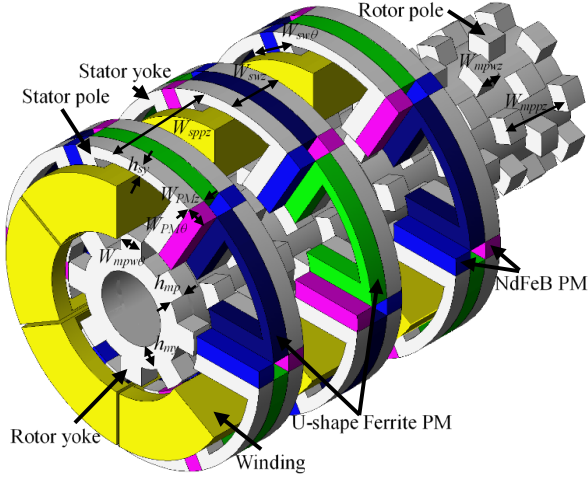

Fig. 1. The topology of an FS-LRPMM

TABLE I. VARIATION RANGES OF DESIGN PARAMETERS

Design parameters	Variation range
PM width in circumferential direction $W_{PM\theta}$	[3mm,7.5mm]
Ferrite PM width in axial direction W_{FPMz}	[3.5mm,5.25mm]
Mover pole width in axial direction W_{mpwz}	[5mm,7.25mm]
Mover pole width in circumferential direction $W_{mpw\theta}$	[6.4mm,8.4mm]
Stator yoke height h_{sy}	[2.5 mm,7.5mm]
Stator pole pitch in axial direction W_{sppz}	[35 mm,38.5mm]
Stator pole width in axial direction W_{swz}	[4.5mm,8.25mm]
Mover pole pitch in axial direction W_{mppz}	[3.5mm,5.25mm]
Mover yoke height h_{my}	[5 mm,10.5 mm]
Stator pole width in circumferential direction $W_{sw\theta}$	[11mm,17mm]
Mover pole height h_{mp}	[3.9mm,8.4mm]

Since the influences of each design parameters on the optimization objectives are different, the sensitivity analysis method is adopted, and the expressions of the corresponding sensitivity index $S_1(x_i)$, $S_2(x_i)$, $S_3(x_i)$ are

$$s_{avg}(x_i) = 2\sum_{i=1}^{m}\left|\frac{f(x_{i+1})-f(x_i)}{x_{i+1}-x_i}\right|/(m-1) \quad (1)$$

$$s_1(x_i) = s_{avg}(x_i)/(x_{i+1}-x_i) \quad (2)$$

$$s_2(x_i) = s_{avg}(x_i)/Max(f(x_1),f(x_2)...f(x_i)) \quad (3)$$

$$s_3(x_i) = s_{avg}(x_i)/Min(f(x_1),f(x_2)...f(x_i)) \quad (4)$$

where $f(x_i)$ is the optimization objective, $S_{avg}(x_i)$ is the average value of the optimization objective amplitude, and x_i is the selected design parameter, i=1, 2, 3…m.

Based on the theoretical analysis, Fig. 2 illustrates the amplitude waveforms of cogging torque and detent force with the selected eleven design parameters. Table II is the average value of the amplitude of the cogging torque and detent force. It is observed that each design parameter possesses different sensitivities on the different optimization objectives. The analysis is a local sensitivity analysis and it cannot be applied to global space of the input design parameters.
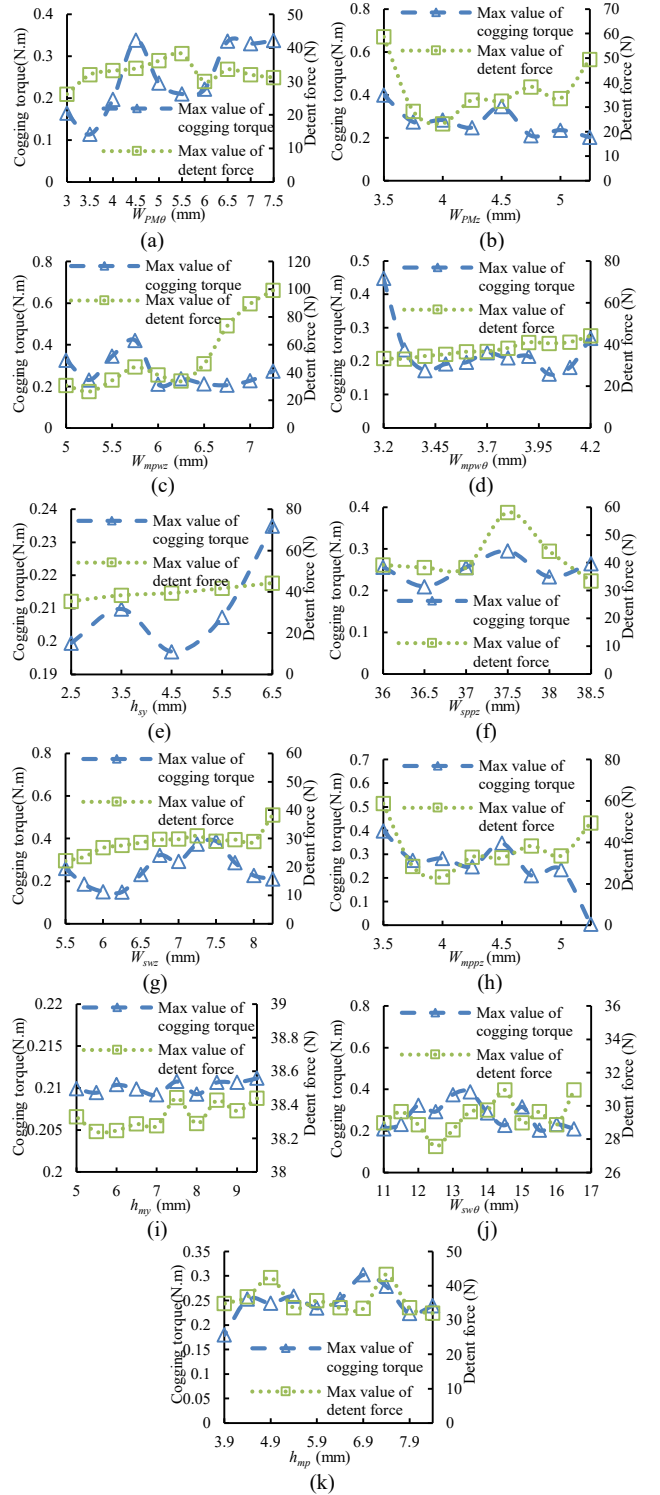

Fig. 2. Amplitude waveforms of cogging torque and detent force of the selected parameters. (a) $W_{PM\theta}$, (b) W_{PMz}, (c) W_{mpwz}, (d)$W_{mpw\theta}$, (e)h_{sy}, (f)W_{sppz}, (g)W_{swz}, (h)W_{mppz}, (i) h_{my}, (j) $W_{sw\theta}$, (k)h_{mp}.

TABLE II. AVERAGE VALUE OF THE AMPLITUDE OF COGGING TORQUE AND DETENT FORCE

Parameters	Cogging torque (Nm)	Detent force (N)	Parameters	Cogging torque (Nm)	Detent force (N)
$W_{PM\theta}$	0.06	2.95	W_{FPMz}	0.066	10.27
W_{mpwz}	0.069	10.82	$W_{mpw\theta}$	0.05	1.22
h_{sy}	0.015	2.21	W_{sppz}	0.045	9.09
W_{swz}	0.053	1.96	W_{mppz}	0.094	10.28
h_{my}	0.00084	0.082	$W_{sw\theta}$	0.059	1.057
h_{mp}	0.031	4.64	\	\	\

According to the above principle formula, the sensitivity index of each design parameter on two design objectives are figured out and the results are collected in Table III. The design parameter with a relatively high absolute value of the sensitivity factor means the impact of the design parameter on optimization objectives is greater than others.

TABLE III. SENSITIVITY OF DESIGN PARAMETERS

Parameters	Cogging torque			Detent force		
	$S_1(x_i)$	$S_2(x_i)$	$S_3(x_i)$	$S_1(x_i)$	$S_2(x_i)$	$S_3(x_i)$
$W_{PM\theta}$	0.24	0.43	10.39	11.82	0.35	4.16
W_{FPMz}	0.26	0.48	7.41	41.1	0.34	23.74
W_{mpwz}	0.27	0.32	11.37	43.29	0.40	2.50
$W_{mpw\theta}$	0.51	0.24	9.81	12.25	0.41	8.95
h_{sy}	0.015	0.55	1.479	2.21	0.76	2.05
W_{sppz}	0.09	0.72	1.43	18.18	0.46	1328.06
W_{swz}	0.21	0.53	32.59	7.86	0.21	20.27
W_{mppz}	0.38	0.41	10.84	41.13	0.34	22.72
h_{my}	0.0017	0.52	289.94	0.16	0.49	11.50
$W_{sw\theta}$	0.23	0.53	4.43	4.23	0.50	10.89
h_{mp}	0.063	0.073	0.0083	9.27	9.89	0.23

By taking the computational process of $W_{PM\theta}$ as an example, Fig. 2(a) shows the waveforms of cogging torque and detent force versus $W_{PM\theta}$. $\Delta W_{PM\theta}$ is 0.25mm, and the sensitivities of the amplitude of the average value are 0.24 and 11.82, respectively, which can be taken as the finial sensitivity. The computation values are listed in table IV.

TABLE IV COMPUTATION VALUES OF COGGING TORQUE AND DETENT FORCE RELATED WITH $W_{PM\theta}$.

Parameters	$W_{PM\theta}$	T_{cog}	F_{det}	ΔT_{cog}	ΔF_{det}	S_{cog}	S_{den}
value	3	0.164	26.14	/	/	0.24	11.82
	3.5	0.11	31.97	-0.054	5.83		
	4	0.197	33.16	0.087	1.19		
	4.5	0.34	33.87	0.143	0.71		
	5	0.236	36.15	-0.104	2.28		
	5.5	0.21	38.29	-0.026	2.14		
	6	0.221	29.94	0.011	-8.35		
	6.5	0.33	33.59	0.109	3.65		
	7	0.33	31.96	0	-1.63		
	7.5	0.34	31.14	0.01	-0.82		

For the proposed FS-LRPMM, the torque/ thrust needs to be the maximal value, while its cogging torque/detent force and torque/thrust ripple should be the lowest values. In order to solve the problem effectively, weight coefficient is applied to evaluate each design parameter considering six optimization goals. The corresponding comprehensive sensitivity function is defined as

$$S_{\text{FS-LRPMM}}(x_i)$$
$$= w_1|S_{Tc}| + w_2|S_{Fd}| + w_3|S_{Tavg}| + w_4|S_{Tr}| + w_5|S_{Favg}| + w_6|S_{Fr}| \quad (5)$$

where $S_{\text{FS-LRPMM}}(x_i)$ is the sensitivity function of the machine, S_{Tc}, S_{Fd}, S_{Tavg}, S_{Tr}, S_{Favg} and S_{Fr} are the sensitivity of cogging torque, detent force, average torque, torque ripple, average thrust and thrust ripple, respectively. w_1, w_2, w_3, w_4, w_5, w_6 are the weights of the six objectives, which can be determined by the specific design requirements for the optimization objectives, and they satisfy $w_1+w_2+w_3+w_4+w_5+w_6=1$. In the process of multi-objective optimization, the selection of weight factors is very important. According to the analysis above, the variation of the thrust and thrust ripple is relatively small when the parameter is changed. Hence, the

values of w_5 and w_6 are selected as 0.1. The coefficients w_1, w_2, w_3, w_4 are selected to be 0.2.

III. OPTIMIZATION DESIGN AND RESULTS

A. Traditional response surface method

The traditional RSM is always used to find the relationship between design parameters and responses. The second-order regression model of response surface is expressed as:

$$f = \beta_0 + \sum_{i=1}^{k}\beta_i z_i + \sum_{i=1}^{k}\beta_{ii}z_i^2 + \sum_{i=1}^{k-1}\sum_{j=1}^{k}\beta_{ij}z_i z_j + \sigma \quad (6)$$

where f is the predicted value of any one of the six design objectives and k is the number of design parameters. σ is a term representing sources of variability not accounted for in f, which is treated as a statistical error. β_0, β_i, β_j and β_{ij} are regression coefficients. z_i and z_j means two different optimization parameters which means different combinations of product-term of two parameters.

B. Initial Analysis

Based on the statistical fitting method and the observed data calculated by 2-D FEM as shown in Fig. 2, the independent parameters are changed within a small interval, and the fitting functions of cogging torque and detent force related with $W_{PM\theta}$, W_{PMz}, W_{mpwz}, $W_{mpw\theta}$, h_{sy}, W_{sppz}, W_{swz}, W_{mppz}, h_{my}, $W_{sw\theta}$, h_{mp} can be expressed by the fitting of Fourier transform and low-order polynomial.

The expressions of cogging torque T_{c1} and T_{c2} can be expressed as

$$T_{c1}(a_{c0}, a_{ck}, b_{ck}, w_c, x, n) = a_{c0} + \sum_{k=1}^{n} a_{ck}\cos kw_c x + b_{ck}\sin kw_c x \quad (7)$$

$$T_{c2}(p_{c1}, p_{c2}, p_{c3}, p_{c4}, ... x, n) = p_{c1}x + p_{c2}x^2 + p_{c3}x^3 + ... \quad (8)$$

The functions of cogging torque related with $W_{PM\theta}$, W_{mpwz}, $W_{mpw\theta}$, W_{swz}, W_{mppz}, h_{my}, $W_{sw\theta}$, h_{mp} can be expressed as

$$T_{c1\_W_{PM\theta}} = T_{c1}(a_{c0\_W_{PM\theta}}, a_{ck\_W_{PM\theta}}, b_{ck\_W_{PM\theta}}, w_{c\_W_{PM\theta}}, W_{PM\theta}, 3) \quad (9)$$

$$T_{c1\_W_{mpwz}} = T_{c1}(a_{c0\_W_{mpwz}}, a_{ck\_W_{mpwz}}, b_{ck\_W_{mpwz}}, w_{c\_W_{mpwz}}, W_{mpwz}, 3) \quad (10)$$

$$T_{c1\_W_{mpw\theta}} = T_{c1}(a_{c0\_W_{mpw\theta}}, a_{ck\_W_{mpw\theta}}, b_{ck\_W_{mpw\theta}}, w_{c\_W_{mpw\theta}}, W_{mpw\theta}, 3) \quad (11)$$

$$T_{c1\_W_{swz}} = T_{c1}(a_{c0\_W_{swz}}, a_{ck\_W_{swz}}, b_{ck\_W_{swz}}, w_{c\_W_{swz}}, W_{swz}, 3) \quad (12)$$

$$T_{c1\_W_{mppz}} = T_{c1}(a_{c0\_W_{mppz}}, a_{ck\_W_{mppz}}, b_{ck\_W_{mppz}}, w_{c\_W_{mppz}}, W_{mppz}, 3) \quad (13)$$

$$T_{c1\_h_{my}} = T_{c1}(a_{c0\_h_{my}}, a_{ck\_h_{my}}, b_{ck\_h_{my}}, w_{c\_h_{my}}, h_{my}, 4) \quad (14)$$

$$T_{c1\_W_{sw\theta}} = T_{c1}(a_{c0\_W_{sw\theta}}, a_{ck\_W_{sw\theta}}, b_{ck\_W_{sw\theta}}, w_{c\_W_{sw\theta}}, W_{sw\theta}, 4) \quad (15)$$

$$T_{c1\_h_{mp}} = T_{c1}(a_{c0\_h_{mp}}, a_{ck\_h_{mp}}, b_{ck\_h_{mp}}, w_{c\_h_{mp}}, h_{mp}, 4) \quad (16)$$

The functions of cogging torque related with W_{FPMz}, h_{sy}, W_{sppz} can be expressed as

$$T_{c2\_W_{FPMz}} = T_{c2}(p_{c1\_W_{FPMz}}, p_{c2\_W_{FPMz}}, p_{c3\_W_{FPMz}}...p_{c6\_W_{FPMz}}, W_{FPMz}, 8) \quad (17)$$

$$T_{c2\_h_{sy}} = T_{c2}(p_{c1\_h_{sy}}, p_{c2\_h_{sy}}, p_{c3\_h_{sy}}, p_{c4\_h_{sy}}, h_{sy}, 4) \quad (18)$$

$$T_{c2\_W_{sppz}} = T_{c2}(p_{c1\_W_{sppz}}, p_{c2\_W_{sppz}}, p_{c3\_W_{sppz}}, p_{c4\_W_{sppz}}, W_{sppz}, 4) \quad (19)$$

Tables V and VI list the coefficients values of cogging torque T_{c1} and T_{c2} calculated by 2-D FEM.

TABLE V. COEFFICIENT VALUES OF COGGING TORQUE T_{C1} FUNCTION

	$W_{PM\theta}$	W_{mpwz}	$W_{mpw\theta}$	W_{swz}	W_{mppz}	h_{my}	$W_{sw\theta}$	h_{mp}
a_{c0}	0.257	-26220	0.9006	0.256	$-1.283*10^8$	0.2101	0.2777	-12630
a_{c1}	0.02112	7352	-0.6189	-0.08553	$1.805*10^8$	$2.492*10^4$	-0.03446	20460
b_{c1}	0.06113	38830	0.9321	0.03568	$6.683*10^7$	$2.943*10^4$	0.0616	278.1
a_{c2}	-0.05684	14920	-0.2121	-0.005824	$-5.847*10^7$	$6.711*10^7$	-0.02059	-10620
b_{c2}	-0.03872	-5858	-0.4935	-0.03214	$-5.018*10^7$	$-2.01*10^4$	-0.005653	-285.8
a_{c3}	-0.02195	-1455	0.09776	-0.03595	$6.243*10^6$	$-5.113*10^4$	0.02038	3227
b_{c3}	0.04244	-2317	0.01431	-0.0004099	$1.124*10^7$	$-1.229*10^4$	0.01084	128
a_{c4}	0	0	0	0	0	$2.88*10^4$	-0.03689	-440.4
b_{c4}	0	0	0	0	0	$-4.439*10^4$	0.002378	-22.59
w_c	2.182	0.3171	3.101	2.081	0.08192	1.375	2.217	-0.3929

TABLE VI. COEFFICIENT VALUES OF COGGING TORQUE T_{C2} FUNCTION

	p_{c1}	P_{c2}	P_{c3}	p_{c4}	p_{c5}	p_{c6}
W_{FPMz}	-15.96	487.3	-6358	45940	-198500	513200
h_{sy}	0.003379	-0.4824	22.95	-363.7	0	0
W_{sppz}	0.003379	-0.4824	22.95	-363.7	0	0

In a similar way, the expressions of the amplitude of the detent force F_{d1} and F_{d2} can be expressed as

$$F_{d1}(a_{d0},a_{dk},b_{dk},w_d,x,n)=a_{d0}+\sum_{k=1}^{n} a_{dk}\cos kw_d x + b_{dk}\sin kw_d x$$

(20)

$$F_{d2}(p_{d1},p_{d2},p_{d3},p_{d4},...x,n)=p_{d1}x + p_{d2}x^2 + p_{d3}x^3 +... \quad (21)$$

Then the functions of the amplitude of the detent force related with $W_{PM\theta}$, W_{PMz}, W_{mpwz}, $W_{mpw\theta}$, W_{swz}, W_{mppz}, h_{my}, $W_{sw\theta}$, h_{mp} can be expressed by (20) and related with h_{sy}, W_{sppz} can be expressed by (21), which are calculated based on the analyze results by 2-D FEM.
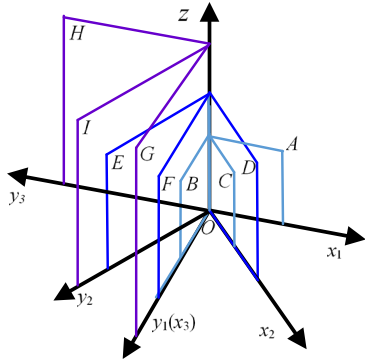
C. Coordinate System Conversion


Fig. 3. Coordinate systems

Fig. 3 shows the coordinate systems, which can make the selected parameters relate with each other. The core idea of the improved method is to transform two waveforms into a third coordinate system, then reconstruct a new waveform by defining a virtual x coordinate and incorporate the previous two waveforms. Firstly, make the x-axis coordinate values into standard values. Since multi-parameters are mutually influential, assume that the waveform related with the first parameter and the second parameter is shown in the 3-D coordinate system (x_1, y_1, z), then transform the 3-D waveform into another plane $C(x_2Oz)$ by coordinate transform. Namely, the x-axis coordinate becomes the $\sqrt{2}/2$ the original value, and the waveform in the plane $C(x_2Oz)$ and the waveform related with the third selected parameter in the plane $E(y_2Oz)$ form a new 3-D waveform in the

coordinate system (x_2, y_2, z). The multi-parameter multi-objective optimization is completed through the process loop.

Take $W_{PM\theta}$, W_{FPMz}, $W_{mpw\theta}$ as the first, second and third selected parameters. Table VII lists the amplitude of cogging torque related with $W_{PM\theta}$, W_{FPMz}, $W_{mpw\theta}$ parameters. According to the analysis of Fig. 2, 3 mm is selected as the reference value. S_v is the value after the optimization.

TABLE VII. AMPLITUDE OF COGGING TORQUE RELATED WITH $W_{PM\theta}$, W_{FPMz}, $W_{mpw\theta}$ PARAMETERS
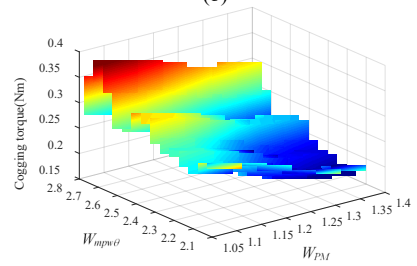
$W_{PM\theta}$	S_v	T_{c1}	W_{FPMZ}	S_v	T_{c1}	$W_{mpw\theta}$	S_v	T_{c1}
3	1	0.16	3.5	1.17	0.4	3	1	0.32
3.5	1.17	0.11	3.75	1.25	0.27	3.2	1.06	0.23
4	1.33	0.2	4	1.33	0.28	3.4	1.13	0.34
4.5	1.5	0.33	4.25	1.42	0.25	3.6	1.2	0.42
5	1.67	0.24	4.5	1.5	0.35	3.8	1.27	0.21
5.5	1.83	0.21	4.75	1.58	0.21	4	1.33	0.24
6	2	0.22	5	1.67	0.24	4.2	1.4	0.212
6.5	2.17	0.34	5.25	1.75	0.2	4.4	1.47	0.206
7	2.33	0.33	/	/	/	/	/	/
7.5	2.5	0.34	/	/	/	/	/	/
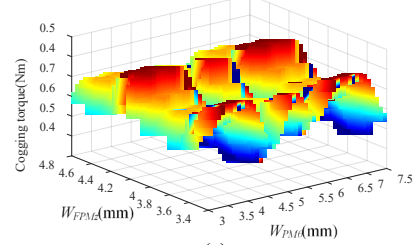
(a)
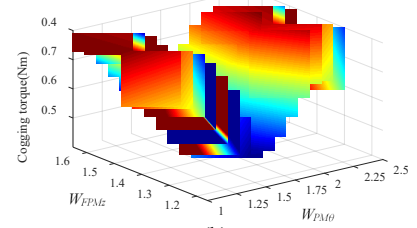
(b)

(c)

Fig. 4. Cogging torque waveforms, (a) waveform related with $W_{PM\theta}$ and W_{FPMz}, (b) standardization waveform, and (c) standardization waveform related with W_{PM} and $W_{mpw\theta}$.

Fig. 4 plots the cogging torque waveforms, which can show the coordinates transformation process clearly. Fig. 4(a) shows the cogging torque waveforms related with $W_{PM\theta}$, W_{FPMz}, and Fig. 4(b) shows the result after the standardization, namely, it is transformed to a 2-D waveform with a virtual parameter W_{PM}, which can reflect the change with $W_{PM\theta}$ and W_{FPMz}. Fig. 4(c) shows the 3-D cogging torque waveform related with $W_{mpw\theta}$ and W_{PM}. It is notable that the design efficiency is improved by incorporating the multi-parameters in the optimization process and decreasing the number of design parameters.

D. Construsting Response Surface Model

When all design parameters are investigated simultaneously, the whole design optimization process will be time-consuming. In order to improve the actual performance of FS-LRPMM and meet the requirements of precision, considering that some design parameters possess large effect on design objectives, the RSM is applied to conduct the optimization based on the detailed analysis of the variation relationships between the design parameters and objectives. The cogging torque optimization is taken as the analysis objective, According to above investigation and the ranges of the optimization parameters, the design parameters ($W_{PM\theta}$, W_{PMz}, W_{mpwz}, $W_{mpw\theta}$, h_{sy}, W_{swz}, W_{mppz}, h_{my}, h_{mp}) are transformed to one virtual parameters (V_i) and the other design parameters (W_{sppz}, $W_{sw\theta}$) are transformed to another one (V_j). and the second-order regression model of response surface is expressed as:

$$f = \beta_0 + \beta_1 V_1 + \beta_2 V_2 + \beta_{11} V_1^2 + \beta_{22} V_2^2 + \beta_{12} V_1 V_2 \quad (20)$$

Taking the data calculated by 2-D FEM as the sample point, the value of the shape parameter can be obtained, and the undetermined coefficient of the second-order polynomial response surface model is calculated based on the least squares method.

IV. 3-D FEM AND EXPERIMENTAL VERIFICATION

According to the optimization results, a prototype of FS-LRPMM is manufactured and the air-gap flux density, cogging torque and detent force, steady output torque/thrust and torque/thrust ripple of the motor are tested, which are used to verify the correctness of the improved optimization method. Fig. 5 shows the prototype of the machine. In order to reduce magnetic flux leakage, the Ferrite PM in the stator yoke has been divided into three sections.
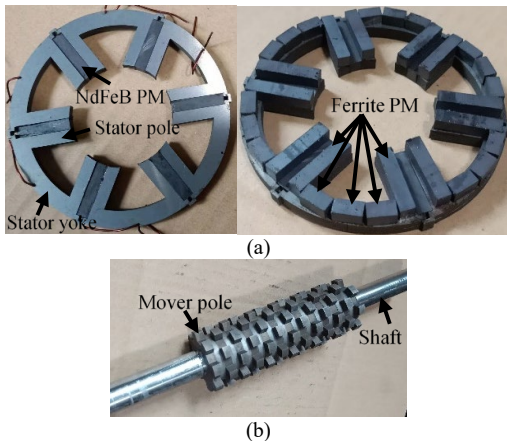

Fig. 5. Prototype of FS-LRPMM: (a) stator, and (b) mover.

A. Air-gap Flux Density Waveform

Fig. 6 shows the air-gap flux density waveforms in radial direction before and after the optimization, which are analyzed by 3-D FEM. It can be observed that the peak value of the air-gap flux density reaches nearly 1.3 T after the optimization in circumferential and axial directions.
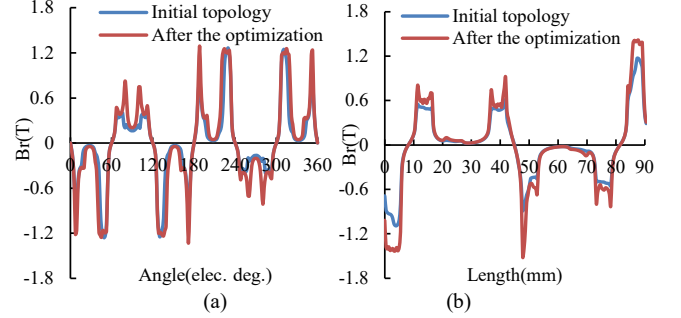

Fig. 6. Air-gap flux density waveforms in radial direction before and after the optimization: (a) in the circumferential direction, and (b) in the axial direction.

B. Cogging Torque and Detent Force Analysis

Fig. 7 shows the cogging torque and detent force waveforms of the prototype before and after the optimization. It is noted that the amplitudes of the cogging torque and detent force are reduced significantly after the optimization.
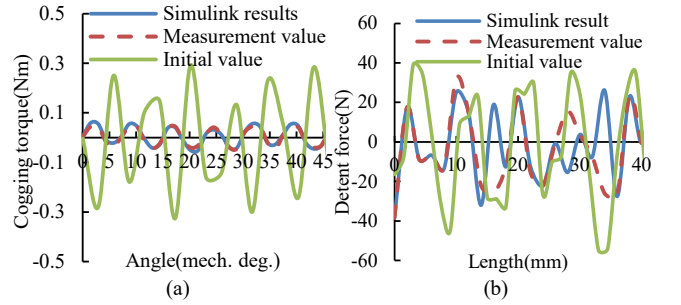

Fig. 7. The cogging torque and detent force waveforms before and after the optimization topology, (a) cogging torque, (b) detent force.

C. Torque and Thrust Performances

When the rated current is 10 A, the rated rotary speed is 1200 rpm and the linear speed is 0.002 m/s, the steady torque and thrust are depicted in Fig. 8. It is noted that the measured torque, torque ripple, thrust and thrust ripple waveforms of the machine are 5.15Nm, 25.3%, 4.94N, 32.4%, respectively. Compared with the initial topology, the electromagnetic characteristic of the machine are improved significantly, the measured waveforms exhibit a good consistency with the simulated waveforms. Since there are machining errors, the measured torque value is a little smaller than the Simulink result and the measured torque ripple is a little higher than the Simulink result, which are within the acceptable range. Compared with the initial model, the optimized average torque and thrust of the Simulink result and experimental test are increased by approximately 128%, 123%, 194%, and 178%, respectively. The optimized torque/thrust ripple are decreased by 48.9%, 46.2%, 73.6% and 78.6%, respectively. The analysis results confirm that the improved method is effective. Table VIII lists the comparison of torque, torque ripple, thrust and thrust ripple before and after the optimization.
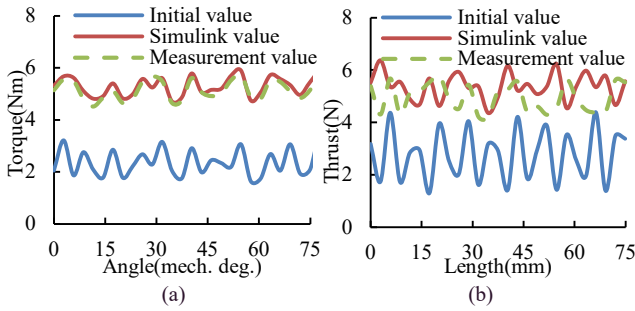
Fig. 8. The comparison waveforms of Torque/thrust, (a) torque waveforms, (b) thrust waveforms.

TABLE VIII. COMPARISON OF TORQUE, TORQUE RIPPLE, THRUST AND THRUST RIPPLE BEFORE AND AFTER THE OPTIMIZATION

Target	Before optimization	After optimization
T(Nm)	2.31	5.26
T_r(%)	71.5	22.6
F(N)	4.16	5.37
F_r(%)	111	37.4

V. CONCLUSIONS

In the paper, an FS-LRPMM is proposed, which has high torque/thrust density. In order to obtain the optimal values of the electromagnetic and structure parameters, a multi-parameter multi-objective optimization method is adopted by converting the selected optimization parameters to two virtual parameters. Then the optimization results can be obtained by RSM. Compared with the non-optimized initial topology, the average torque and thrust are increased by 128% and 29%, respectively. The torque and thrust ripples are decreased by 48.9% and 73.6% after the optimization, which are verified by 3-D FEM and prototype experiments. It is obvious that the proposed method for FS-LRPMM can obtain the optimal design conveniently and efficiently which improves the overall electromagnetic performances of the motor and significantly reduces the computational cost and optimization time.

REFERENCES

[1] X. Zhu, J. Huang, L. Quan, Z. Xiang, and B. Shi, "Comprehensive sensitivity analysis and multiobjective optimization research of permanent magnet flux-intensifying motors," *IEEE Trans. Ind. Electron.*, vol. 66, no. 4, pp. 2613-2627, Apr. 2019.

[2] J. Song, F. Dong, J. Zhao, H. Wang, Z. He, and L. Wang, "An efficient multiobjective design optimization method for a PMSLM based on an extreme learning machine," *IEEE Trans. Ind. Electron.*, vol. 66, no. 2, pp. 1001-1011, Feb. 2019.

[3] S. Wu, X. Zhao, Z. Jiao, P. C. Luk, and C. Jiu, "Multi-objective optimal design of a toroidally wound radial-flux halbach permanent magnet array limited angle torque motor," *IEEE Trans. Ind. Electron.*, vol. 64, no. 4, pp. 2962-2971, Apr. 2017.

[4] G. Cvetkovski, and L. Petkovska, "Multi-objective optimal design of permanent magnet disc motor using cuckoo search," *IEEE Eurocon*, 2017, Jul. 2017.

[5] H. Chen, W. Yan, J. J. Gu, and M. Sun, "Multiobjective optimization design of a switched reluctance motor for low-speed electric vehicles with a taguchi-cso algorithm," *IEEE/ASME Trans. on Mech.*, vol. 23, no. 4, pp. 1762-1774, Aug. 2018.

[6] R. Ilka, Y. Alinejad-Beromi, and H. Yaghobi, "Techno-economic design optimisation of an interior permanent-magnet synchronous motor by the multi-objective approach," *IET Elect. Power Appl.*, vol. 12, no. 7, pp. 972-978, Aug. 2018.

[7] J. Gao, L. Dai, and W. Zhang, "Improved genetic optimization algorithm with subdomain model for multi-objective optimal design of SPMSM," *CES Trans. Elect. Mach. Syst.*, vol. 2, no. 1, pp. 160-165, Mar. 2018.

[8] H. Park, H. Yeo, S. Jung, T. Chung, J. Ro, and H. Jung, "A robust multimodal optimization algorithm based on a sub-division surrogate model and an improved sampling method," *IEEE Trans. Magn.*, vol. 54, no. 3, Art. 8201704, Mar. 2018.

[9] Y. Li, D. Bobba, and B. Sarlioglu, "Design and optimization of a novel dual-rotor hybrid PM machine for traction application," *IEEE Trans. Ind. Electron.*, vol. 65, no. 2, pp. 1762-1771, Feb. 2018.

[10] C. T. Krasopoulos, I. P. Armouti, and A. G. Kladas, "Hybrid multiobjective optimization algorithm for PM motor design," *IEEE Trans. Magn.*, vol. 53, no. 6, Art. 8104304, Jun. 2017.

[11] A. J. Sorgdrager, R. Wang, and A. J. Grobler, "Multiobjective design of a line-start PM motor using the taguchi method," *IEEE Trans. Ind. Appl.*, vol. 54, no. 5, pp. 4167-4176, Sept. 2018.

[12] F. Dong, J. Song, J. Zhao, and J. Zhao, "Multi-objective design optimisation for PMSLM by FITM," *IET Elect. Power Appl.*, vol. 12, no. 2, pp. 188-194, Feb. 2018.

[13] W. Zhao, A. Ma, J. Ji, X. Chen, and T. Yao, "Multi-objective optimization of a double-side linear vernier PM motor using response surface method and differential evolution," *IEEE Trans. Ind. Electron.*, IEEE Early Access, Jan. 2019.

[14] X. Liu, and W. N. Fu, "A dynamic dual-response-surface methodology for optimal design of a permanent-magnet motor using finite-element method," *IEEE Trans. Magn*, vol. 52, no. 3, Art. 7204304, Mar. 2016.

[15] H. M. Hasanien, A. S. Abd-Rabou, and S. M. Sakr, "Design optimization of transverse flux linear motor for weight reduction and performance improvement using response surface methodology and genetic algorithms," *IEEE Trans. Energ. Convers.*, vol. 25, no. 3, pp.598-605, Sept. 2010.

[16] H. A. Moghaddam, A. Vahedi, and S. H. Ebrahimi, "Design optimization of transversely laminated synchronous reluctance machine for flywheel energy storage system using response surface methodology," *IEEE Trans. Ind. Electron.*, vol. 64, no. 12, pp.9748-9757, Dec. 2017.

[17] Z. Gaing, C. Lin, M. Tsai, M. Hsieh, and M. Tsai, "Rigorous design and optimization of brushless PM motor using response surface methodology with quantum-behaved PSO operator," *IEEE Trans. Magn*, vol. 50, no. 1, Art. 4002704, Jan. 2014.

[18] J. Zhu, S. Li, D. Song, Q. Han, J. Wang, and G. Li, "Multi-objective optimisation design of aircored axial flux PM generator," *IET Elect. Power Appl*.

[19] J. Si, S. Zhao, H. Feng, R. Cao, and Y. Hu, "Multi-objective optimization of surface-mounted and interior permanent magnet synchronous motor based on taguchi method and response surface method,". *Chinese Journal of Electrical Engineering*, vol.4, no.1, pp. 67-73, Mar. 2018.

[20] Z. Xiang, X. Zhu, L. Quan, and D. Fan, "Optimization design and analysis of a hybrid permanent magnet flux-switching motor with compound rotor configuration,". *CES Trans. Elect. Mach. Syst.*, vol. 2, no. 2, pp. 200-206, Jun. 2018.

[21] K. Guo, and Y. Guo, "Key parameter design and analysis of flux reversal linear rotary permanent magnet actuator," *IEEE Trans. Appl. Supercond.*, vol. 29, no. 2, Art: 0600405, Mar. 2019.